Impact of remote oceanic forcing on Gulf of Alaska sea levels and mesoscale circulation

Arne Melsom
Norwegian Meteorological Institute, Oslo, Norway

E. Joseph Metzger and Harley E. Hurlburt
Oceanography Division, Naval Research Laboratory, Stennis Space Center, Mississippi, USA

Received 12 December 2002; revised 18 August 2003; accepted 2 September 2003; published 8 November 2003.

[1] We examine the relative importance of regional wind forcing and teleconnections by an oceanic pathway for impact on interannual ocean circulation variability in the Gulf of Alaska. Any additional factors that contribute to this variability, such as freshwater forcing from river runoff, are disregarded. The study is based on results from numerical simulations, sea level data from tide gauge stations, and sea surface height anomalies from satellite altimeter data. At the heart of this investigation is a comparison of ocean simulations that include and exclude interannual oceanic teleconnections of an equatorial origin. Using lagged correlations, the model results imply that 70–90% of the interannual coastal sea level variance in the Gulf of Alaska can be related to interannual sea levels at La Libertad, Equador. These values are higher than the corresponding range from sea level data, which is 25–55%. When oceanic teleconnections from the equatorial Pacific are excluded in the model, the explained variance becomes about 20% or less. During poleward propagation the coastally trapped sea level signal in the model is less attenuated than the observed signal. In the Gulf of Alaska we find well-defined sea level peaks in the aftermath of El Niño events. The interannual intensity of eddies in the Gulf of Alaska also peaks after El Niño events; however, these maxima are less clear after weak and moderate El Niño events. The interannual variations in eddy activity intensity are predominantly governed by the regional atmospheric forcing. *INDEX TERMS:* 4556 Oceanography: Physical: Sea level variations; 4516 Oceanography: Physical: Eastern boundary currents; 4520 Oceanography: Physical: Eddies and mesoscale processes; 4522 Oceanography: Physical: El Niño; *KEYWORDS:* oceanic teleconnections, remote forcing, interannual variability

Citation: Melsom, A., E. J. Metzger, and H. E. Hurlburt, Impact of remote oceanic forcing on Gulf of Alaska sea levels and mesoscale circulation, *J. Geophys. Res.*, *108*(C11), 3346, doi:10.1029/2002JC001742, 2003.

1. Introduction

[2] Variability related to the El Niño/Southern Oscillation (ENSO) may affect the extratropical oceans in two ways. First, the local surface winds may be remotely forced by an atmospheric link to the tropical Pacific Ocean [*Bjerknes*, 1966; *Emery and Hamilton*, 1985]. Second, the extratropical oceans may be affected via tropically generated oceanic anomalies, such as planetary waves [*Johnson and O'Brien*, 1990] and coastally trapped waves [*Enfield and Allen*, 1980].

[3] Coastally trapped waves such as Kelvin waves will occur whenever there is a convergence or divergence of mass along a coastline. Such anomalies may be generated by the local winds, or ocean transients that impact the coastline. Similar effects, including Kelvin waves, can be observed in the ocean along the equator, which is another oceanic wave guide. Large amplitude equatorial Kelvin waves like those associated with ENSO events can reach the eastern boundary and generate coastally trapped waves that propagate poleward in both hemispheres along the eastern ocean margin [e.g., *Chelton and Enfield*, 1986]. Both equatorial and coastal Kelvin waves are well described in a linear framework, and they are well reproduced in numerical models, even by relatively coarse grids [*Hsieh et al.*, 1983; *O'Brien and Parham*, 1992].

[4] Analysis of ocean temperature and sea level (SL) data has shown that coastally trapped waves generated during El Niño events can propagate from the Pacific coast of equatorial South America up the west coast of North America to the Aleutian Island Chain [*Meyers et al.*, 1998]. *Ramp et al.* [1997] showed that SL anomalies off California during the 1991–1992 El Niño were influenced by a northward propagating signal originating in the Tropics and a southward directed signal originating in the Gulf of Alaska (GoA). The former was attributed to a coastally trapped wave and the latter to regional wind forcing.

[5] The ocean circulation in the GoA is defined by the cyclonic motion in the Pacific subpolar gyre (the Alaska

0148-0227/03/2002JC001742$09.00

Gyre). On the eastern side of the gyre, the Alaska Current flows northward as the extension of the North Pacific Current. The Alaska Current is a broad and weak eastern boundary current that becomes narrower and stronger as it approaches the northern GoA. In a region near the apex of the GoA, the Alaska Current turns into an intense southwestward flowing western boundary current known as the Alaskan Stream.

[6] There is a wave guide at the eastern margin of the GoA where the flow is highly variable because of variations in wind forcing and coastally trapped waves propagating in from the south [*Chelton and Enfield*, 1986; *Melsom et al.*, 1999]. The waveguide provides an oceanic teleconnection pathway for the GoA, giving rise to remotely forced variability. Furthermore, studies have also found that the atmospheric circulation in the GoA is intensified during El Niño conditions, suggesting an atmospheric teleconnection that yields similar results along the coast as downwelling coastally trapped waves [*Okkonen et al.*, 2001]. It has been reported that SL anomalies induced by such atmospheric forcing, can take the form of a signal that is seen to propagate southward along the coastline [*Ramp et al.*, 1997; *Subbotina et al.*, 2001].

[7] The ocean circulation in the interior of the GoA is influenced by eddies which form in the wave guide region and propagate westward. As reported in the literature, large eddies with anticyclonic motion are abundant in this region [*Tabata*, 1982; *Thomson and Gower*, 1998; *Melsom et al.*, 1999; *Murray et al.*, 2001]. *Tabata* [1982] infers that these eddies may have a lifespan of more than one year. *Matthews et al.* [1992] found large eddies similar to those inferred from in situ observations using data from the Geosat geodetic mission. Data from more recent altimeters have proven that the large anticyclonic eddies in the GoA may remain intact for a period well beyond 1 year [*Crawford and Whitney*, 1999; *Okkonen et al.*, 2001]. These eddies can also be observed in infrared radiometer images from satellites [*Thomson and Gower*, 1998], but winter conditions in the GoA generally present few cloud-free days.

[8] Variations in ocean circulation take place on a variety of timescales. In the GoA, there is a significant seasonal variability which is attributed to the atmospheric shift from a winter low to a summer high [e.g., *Royer*, 1975]. This shift is accompanied by a corresponding seasonal variation in the oceanic Ekman transport. Evidence also exists for GoA variability on interannual timescales, from examination of in situ observations [*Emery and Hamilton*, 1985] as well as remote sensing data [*Bhaskaran et al.*, 1993]. *Emery and Hamilton* [1985] related the oceanic interannual variability in the GoA to interannual variations in the regional atmospheric circulation. On still longer timescales, decadal variations were reported by *Lagerloef* [1995] in a study of dynamic topography based mostly on expendable bathythermograph data. *Lagerloef* [1995] attributed this variability to changes in the strength and position of the Aleutian low.

[9] One motivation of our study has been the conflicting reports that exist on how far the ENSO induced coastally trapped signals can propagate along the coastline of the Americas. For the annual and higher frequencies, a number of studies have concluded that this propagation terminates off the coast of California [e.g., *Subbotina et al.*, 2001]. However, this conclusion does not necessarily apply to lower frequencies [e.g., *Chelton and Davis*, 1982]. If coastally trapped signals of an equatorial origin propagate into the GoA, ENSO may also affect the variability of the mesoscale circulation in the GoA [*Melsom et al.*, 1999]. The alternative hypothesis is that the mesoscale variability results from boundary currents driven by coastal Ekman pumping which occurs when "winter wind-stress curl along the coast and immediately seaward of the shelf break is both anomalously negative and meridionally extensive" and by coastal Ekman convergence that occurs when there is a strong northwestward (along-shore) winter wind stress [*Okkonen et al.*, 2001]. We investigate these issues using results from simulations with a large-scale, wind-driven ocean circulation model. The model results are validated by tide gauge station records and satellite altimeter data.

[10] The model results presented here are from the Naval Research Laboratory (NRL) Layered Ocean Model (NLOM). Pacific NLOM and its basic characteristics were described in detail by *Hurlburt et al.* [1996]. NLOM has previously been used for a number of large-scale eddy-resolving experiments, including investigations of remote oceanic anomalies due to El Niño events [*Jacobs et al.*, 1994; *Melsom et al.*, 1999]. Here interannual simulations (1979–1999) with two NLOM domains are used to isolate and quantitatively measure the impact of ENSO-related oceanic teleconnections on GoA variability, both along the GoA coastline and in the interior. One domain is the standard Pacific configuration that includes the equatorial latitudes, while the other is designed to prevent propagation of coastally trapped waves from El Niño events into the North Pacific Ocean by excluding latitudes south of 14°N. Model-data comparisons are also used in support of this investigation. Hereafter, when we discuss effects of "remote forcing" (in the GoA), we consider events that are affected by teleconnections with tropical latitudes.

[11] NLOM and the simulations that will be discussed are presented in section 2, and the observational and model records that are analyzed are described in section 3. In section 4, a simple technique is used to distinguish between regions where the variability is a relatively deterministic response to atmospheric forcing (possibly remote), and where it is relatively nondeterministic because of flow instabilities. We present evidence for a significant impact of ENSO events on the interannual sea levels (ISLs) along the coastline of the GoA in section 5. The effects of teleconnections and ENSO events on the sea surface height variability are then discussed in section 6. Finally, the results are summarized and conclusions are drawn in section 7.

2. Ocean Model

[12] The NRL Layered Ocean Model is a primitive equation layered formulation where the dynamic and thermodynamic equations have been vertically integrated through each layer. The six-layer, thermodynamic, finite depth model of the Pacific Ocean used in this study is a descendant of the model by *Hurlburt and Thompson* [1980] with significant enhancements by *Wallcraft* [1991], *Wallcraft and Moore* [1997], and *Moore and Wallcraft* [1998]. Specific details

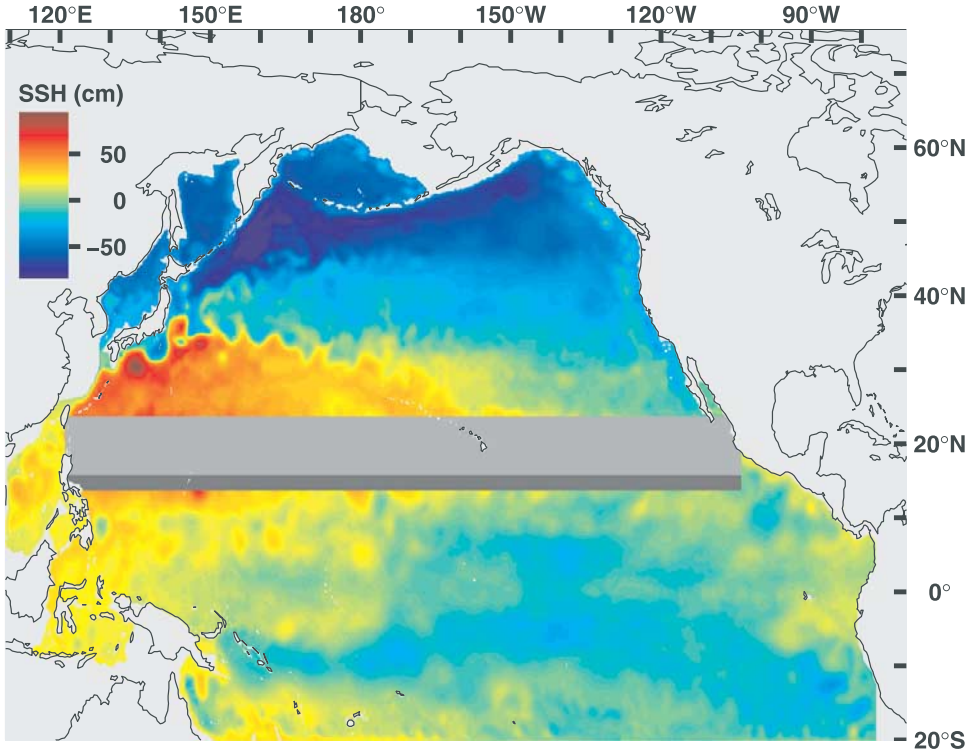

Figure 1. The full domain model covers the Pacific Ocean north of 20°S except regions that are shallower than 200 m. The reduced domain model covers the Pacific Ocean north of 14°N, and the wind forcing has been modified in the medium gray and dark gray areas (between 14°N and 24°N) to minimize artificial generation of intraseasonal Kelvin waves along the artificial boundary at this latitude. The shades of gray have been overlain on a snapshot of the full domain model sea surface height for 30 May 1983. The color scale used for SSH levels is shown by the bar. See the text for further details.

regarding the model equations and parameters are given by *Metzger and Hurlburt* [2001].

[13] Two model subdomains of the Pacific Ocean are used, as presented in Figure 1. The "full domain" model (FDM) is the standard NLOM configuration for the Pacific. It ranges from 20°S to 62°N and 109.125°E to 77.21°W. The initial thicknesses of the five upper layers are 80 m, 140 m, 160 m, 245 m, and 375 m, respectively. The sixth layer extends to the bottom. The reference densities of the six layers (used for the semi-implicit numerical treatment of gravity waves) are 23.56, 25.22, 26.40, 26.96, 27.34 and 27.77 (σ_t, in kg/m^3), respectively. The density climatologies for each layer were determined by iteration, using the mean Levitus climatology for each layer at various stages of the climatologically forced model spin up.

[14] The reduced domain model (RDM) has southern, western and eastern boundaries at 14°N, 121.08°E and 104.07°W, respectively. In the RDM, the southern closed boundary was chosen at 14°N because it is the approximate latitude that separates the subtropical and tropical gyres in the ocean climatology defined by the Navy's Generalized Digital Environmental Model [*Teague et al.*, 1990]. The western boundary in the RDM was chosen to exclude flow into the South China Sea. The initial thicknesses of the five upper layers in the RDM simulation were set to the average layer thicknesses over the reduced domain from a climatologically forced FDM experiment. The initial thicknesses were thus 75 m, 164 m, 144 m, 306 m, and 385 m, respectively. The reference densities of the layers are the same in the FDM and the RDM.

[15] Exclusion of the tropical latitudes south of 14°N in the RDM precludes equatorially generated Kelvin waves from propagating poleward as coastally trapped waves along the America's coast and into the GoA. Thus the RDM eliminates the remote oceanic effects of El Niño events, and calculating FDM minus RDM helps provide a better understanding of how the SL variability in the GoA is affected by equatorial ocean events seen during El Niños and La Niñas. Note that differences between the RDM and the FDM are influenced by oceanic variability from all latitudes that are not included in the RDM, not only teleconnections from the equator.

[16] While the FDM simulations were computed from four different initial states, only one simulation was conducted with the RDM. Results from one of the FDM realizations that was selected randomly from the set of four ensemble members are compared extensively with the RDM results in this study. Results cited in section 4 indicate that a single ensemble member is adequate for comparing FDM and RDM predictions of coastal sea levels. The selected FDM ensemble member for this analysis will hereafter be referred to as FDM-1.

[17] The horizontal resolution of each prognostic model variable is 1/8° in latitude by 45/256° in longitude. A modified version of the 1/12° ETOP05 bottom topography [*National Oceanic and Atmospheric Administration* (*NOAA*),

Table 1. Sea Level Station Metadata[a]

SL Station	Station Position		Model Position		Distance, km	No Data, days
	Longitude	Latitude	Longitude	Latitude		
La Libertad, Ecuador	80°55′W	2°12′S	81°04′W	2°15′S	6	14
Neah Bay, WA	124°37′W	48°22′N	125°32′W	48°15′N	69	114
Sitka, AK	135°21′W	57°03′N	136°06′W	57°00′N	46	3
Kodiak Island, AK	152°31′W	57°44′N	151°33′W	57°00′N	96	48

[a]The positions of the tide gauge stations, the positions of their model representations, and the distance between these positions are listed. The number of days with no observational data during the period 1982–1998 is listed in the rightmost column.

1986] was used in the model. The topography was interpolated to the model grid, then smoothed twice with a nine-point real smoother to reduce topographic energy generation at scales poorly resolved by the model. The 200 m isobath generally defines the model land/sea boundary but there are some exceptions, for example, the Taiwan Strait and the inflow/outflow straits in the Japan/East Sea.

[18] The *Hellerman and Rosenstein* [1983] (HR) monthly mean wind stress climatology is used to spin both models up to statistical equilibrium. This is followed with synoptic forcing by European Centre for Medium-Range Weather Forecasts (ECMWF) 1000 hecto-Pascal (hPa) winds [*ECMWF*, 1995]. The long-term temporal mean of the synoptic winds is replaced by the annual mean from HR as discussed by *Metzger et al.* [1992]. The magnitude (but not direction) of the ECMWF winds is modified to account for the 1000 hPa level not always being at the surface [*Hundermark et al.*, 1999]. The winds are converted to a stress using the density of air (ρ_{air}) = 1.2 kg m^{-3} and a constant drag coefficient (c_d) = 1.5 × 10^{-3}. The model is forced 1979–1993 using the 6-hourly ECMWF reanalysis winds [*Gibson et al.*, 1997] and then continued 1994–1999 using the ECMWF archived operational 12 hourly winds. The reanalysis model had a T106 resolution, whereas the resolution of the operational product during the timeframe after 1993 was at least T213. (T106 and T213 refer to spectral global models which for any latitude are able to produce at most 106 and 213 zonal waves around the globe, respectively.) The switch in ECMWF products across the 1993/1994 time boundary was investigated to make sure no large-scale response might be introduced into the ocean model, and none was found. The ocean model is not forced by atmospheric sea level pressure fields.

[19] To prevent generation of spurious Kelvin waves along the southern boundary in the RDM, the winds were modified as follows. In the band from 14°–16°N (dark gray region in Figure 1), pure HR winds were used; that is, a simple linear interpolation of the monthly HR stresses to 6- or 12-hourly intervals was added to the HR annual mean. In the band between 16° and 24°N (medium gray region in Figure 1) the 6- or 12-hourly ECMWF and interpolated HR products were blended using a cosine-weighted function to minimize spurious wind stress curl at the northern and southern boundary of this blending region and the results were added to the HR mean. North of 24°N the 6- or 12-hourly ECMWF products were added to the HR mean, i.e., identical to the forcing of the FDM. The wind blending technique used for the RDM proved to be effective in eliminating intraseasonal Kelvin wave generation and interannual variability along the southern boundary.

[20] Because of the seasonality of the wind forcing at the southern boundary, a significant annual signal can be observed in the RDM. At 15°N on the eastern boundary, the standard deviation of the daily climatology in the RDM SL results is approximately 11.4 cm. (The daily climatology is represented by one value for each day of the year.) At the same latitude, the FDM has an amplitude of about 3.5 cm. However, as this signal propagates poleward along the coast of Central and North America, its amplitude is significantly reduced. Off the panhandle of Alaska, where seasonal winds reamplify the daily climatology, the SL standard deviations from the RDM and the FDM are around 8 cm and 5.1 cm, respectively.

[21] More than 250 model spin-up years were simulated using the climatological HR forcing, many at coarser horizontal resolution. After spin-up to statistical equilibrium at 1/8° resolution, the simulations were continued with synoptic wind forcing from 1979 onward. Inaccuracies may then exist initially because of the transition from low-frequency to high-frequency atmospheric forcing. In addition, anomalies from climatology that existed at the beginning of 1979 are missing from the climatological initial state. As will become evident from our results, the relevant timescales in our study range from a few months (for signal propagation along the American coastline) to about one year (for advection of eddies into the interior of the GoA). Thus we find that a three year period, from 1979 to 1982, is sufficient for the ocean to adjust to the high-frequency atmospheric forcing. A mismatch between the climatological forcing and the actual conditions in 1979 may lead to a much longer adjustment, and this can potentially give rise to unrealistic trends in the model results, but none were detected in our analysis.

3. Observations and Model Results

[22] Observational records of SLs were obtained from the Research Quality Data Set at the Joint Archive for Sea Level for the four stations listed in Table 1. We note that La Libertad and Sitka have almost complete records of daily SLs for the model integration period. For Neah Bay, the flagged days are in the spring of 1982 and in the falls of 1992 and 1995. The flagged days for Kodiak Island are in February and December of 1994. All missing values were replaced by the daily climatologies, which were determined from years with no missing data. The model integration period extends over more than 6200 days.

[23] La Libertad was chosen because of its equatorial proximity and because of its almost complete record of daily SL observations for the period we study. The obvious

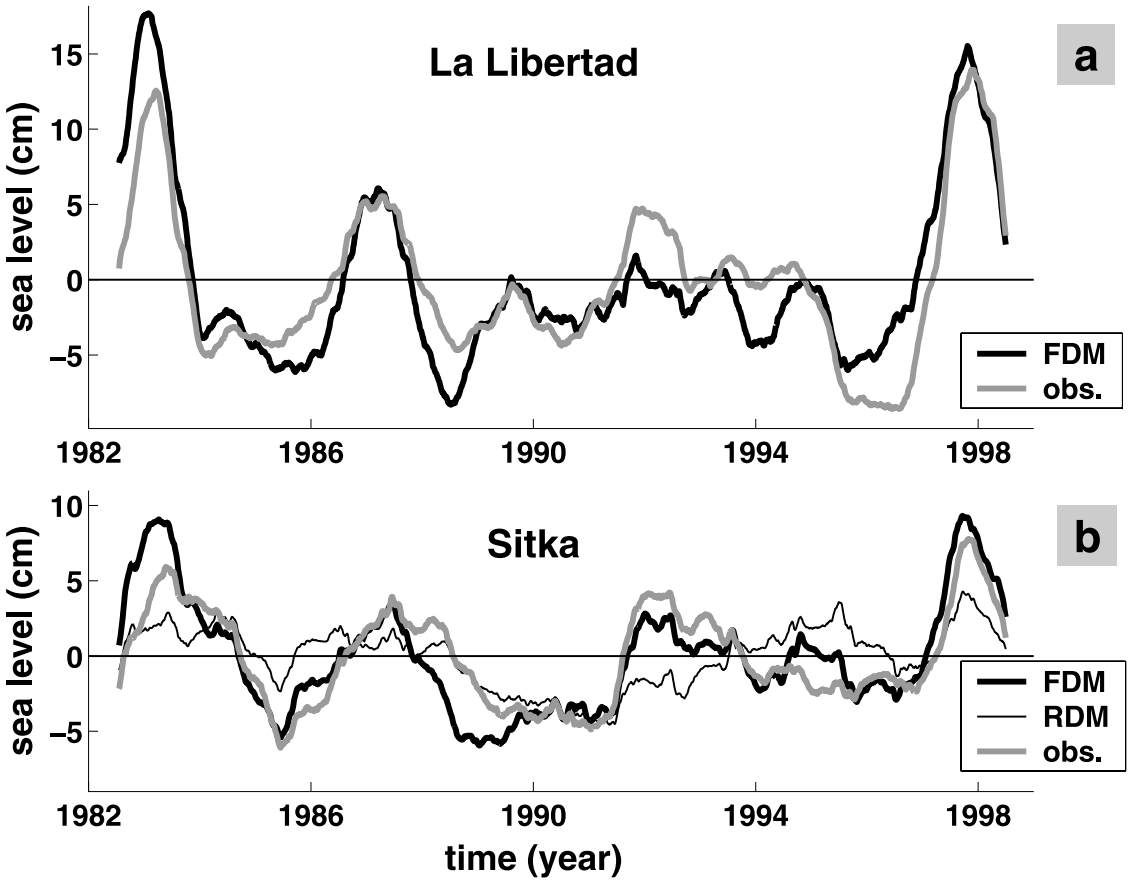

Figure 2. Detrended time series of interannual sea level variations (a) at La Libertad, Ecuador and (b) at Sitka, AK. Thick gray and thick black lines show results from the observational records and from the FDM, respectively. The thin black line in Figure 2b displays the interannual time series from the RDM. A 1-year boxcar filter has been applied to all records. Units of the vertical axis are centimeters. Tick marks on the horizontal axis indicate beginning of years. At La Libertad the correlation and RMS difference between the FDM results and the observations are 0.89 and 2.6 cm, respectively. The corresponding values for Sitka are 0.85 and 1.9 cm. The correlation and RMS difference between the RDM results and the observations for Sitka are 0.54 and 2.4 cm, respectively.

alternative station north of the equator is Buenaventura, Ecuador, but this record includes large gaps during the period under investigation, with a total of 722 days with missing data. (Another alternative station in the Northern Hemisphere, Tumaco, Colombia, has more that 1000 days with missing data.) While a Northern Hemisphere station would be our choice of preference, the SL observations and model results for La Libertad remain adequate measures of mass convergence in the equatorial mixed layer at the American coastline.

[24] The SL data were then corrected for the inverted barometer effect:

$$\zeta_{corr} = \zeta + \frac{\Delta p}{g\rho} \tag{1}$$

where ζ is the observed SL, Δp is the sea level pressure anomaly, and g is the acceleration due to gravity. In this study, the ECMWF sea level pressure product was used for the computation of the corrected SL, ζ_{corr}. Time series of the inverted barometer ($-\Delta p/g\rho$) were also obtained, to facilitate a quantification of any relations between interannual sea level pressure variability in the NeP/GoA and ISL variability along the coast of South America at equatorial latitudes.

[25] In order to examine ISL variability along the rim of the eastern Pacific Ocean in the Northern Hemisphere, time series were stored with a temporal resolution of 3.05 days from the FDM-1 and RDM simulations at the locations listed in Table 1. (Because of the exclusion of the continental shelf in the models, results are not available at the exact locations of the tide gauge stations.) The detrended ISL time series for La Libertad and Sitka are depicted in Figure 2.

[26] Errors in the prescribed atmospheric forcing fields will obviously give rise to discrepancies between model results and observations. This is the case for the coastal winds in the GoA, where orographic effects due to the vicinity of the Rocky Mountains may be inaccurately represented in the atmospheric model. Errors related to aspects of the numerical ocean model formulation may also be significant in this context: Since the continental shelf is not a part of the model, the separation between the tide gauge location and the nearest model grid point can give

rise to sea level differences. (The separation distances are listed in Table 1.) Furthermore, the model shelf break is not realistic. Hence modification of coastally trapped baroclinic waves due to the shelf and shelf break leads to differences between model results and observations. Moreover, variability related to shelf break processes and on-shelf processes such as buoyancy forcing due to freshwater input are not described by the model simulations. Finally, differences in attenuation and dispersion of waves trapped in the coastal wave guide is a potential source of inaccuracy in the model results. Nonetheless, Figure 2 indicates that the model is capable of simulating coastal sea level variability at the selected locations.

[27] Analyzed sea surface height (SSH) data were made available from the Modular Ocean Data Assimilation System (MODAS) [*Fox et al.*, 2002]. The MODAS SSH fields are derived from satellite altimeter data from TOPEX/Poseidon and ERS-2, for the period 1 January 1993 to 31 December 1999. The TOPEX/Poseidon satellite has an along-track resolution of approximately 6 km, and a between-track resolution of about 170 km at the latitudes of the GoA. The corresponding numbers for the ERS-2 satellite are 7 km and 23 km, respectively. The repeat cycles are 10 days for TOPEX/Poseidon and 35 days for ERS-2.

[28] The MODAS SSH product has a temporal resolution of one day, and a meridional and zonal resolution of 0.25°. For this study, SSH fields were interpolated to the model grid. SSH fields are derived by optimal interpolation of the altimeter data, based on the observed covariance of the mesoscale [*Jacobs et al.*, 2001]. Blending data from a relatively coarse spatial resolution and high temporal resolution altimeter (TOPEX/Poseidon) with data from an altimeter with complementary attributes (ERS-2) significantly reduces errors. This principle was demonstrated for the simultaneous use of three instruments by *Jacobs et al.* [2002]. Expected errors are nevertheless relatively high in regions with front or eddy movement that are unresolved by the time and space coverage of the altimeters.

[29] The high-frequency, nonsteric contribution to SSH is not germane to this study. Hence, in the model results it was removed by subtracting the contribution of the abyssal layer pressure field to SSH in post processing. The steric SSH components which remain will be referred to as the baroclinic sea surface height (baroclinic SSH). Moreover, the overall mean value in time at each grid node was removed from the results of both models. Thus the set of baroclinic SSH anomaly fields that are produced by the procedure outlined here are used for analysis in this study.

4. Deterministic Versus Nondeterministic Variability

[30] In order to assess the degree of determinism in the experiments, an ensemble of four FDM simulations was integrated over the period 1979–1996. These simulations differed only in their initial states, which were taken from four different years in the climatological HR model spin-up. Since these simulations differ only in initial state, any differences between them can be attributed to nondeterministic differences in both the initial conditions and the evolution of the simulations. *Metzger et al.* [1994] developed a technique to separate the variability of a variable into two components. The deterministic component is a direct response to atmospheric forcing, whereas the nondeterministic part is due to nonlinear mesoscale flow instabilities. Consider a prognostic variable η which varies in space, and define a partitioning of η by

$$\eta^{n}_{i,j,k}{}^{(s)} = \overline{\eta}_{i,j,k} + \hat{\eta}^{n}_{i,j,k} + \tilde{\eta}^{n}_{i,j,k}{}^{(s)} \tag{2}$$

where *i, j, k* denotes the position in space, *n* corresponds to samples in time, and *s* is a realization in the set of ensemble simulations, which will hereafter be referred to as an ensemble member. If η is a two-dimensional variable, the subscript *k* should be ignored. Further,

$$\overline{\eta}_{i,j,k} = \frac{1}{SN}\sum_{s=1}^{S}\sum_{n=1}^{N}\eta^{n}_{i,j,k}{}^{(s)} \tag{3}$$

is the overall mean value for all S members as a function of space, and

$$\hat{\eta}^{n}_{i,j,k} = \frac{1}{S}\sum_{s=1}^{S}\left[\eta^{n}_{i,j,k}{}^{(s)} - \overline{\eta}_{i,j,k}\right] \tag{4}$$

is the mean offset among the S members from $\overline{\eta}$ as a function of time. Then, from equation (2) we see that $\tilde{\eta}$ is the departure of each member from the instantaneous ensemble mean as a function of space and time so that

$$\sum_{s=1}^{S}\tilde{\eta}^{n}_{i,j,k}{}^{(s)} = 0 \tag{5}$$

[31] Using equations (2) and (4), the variance (σ^2_η) of the anomaly of η may be expressed as

$$\sigma^2_\eta = \frac{1}{SN}\sum_{n=1}^{N}\sum_{s=1}^{S}\left[\eta^{n}_{i,j,k}{}^{(s)} - \overline{\eta}_{i,j,k}\right]^2 = \overline{\hat{\eta}^{n}_{i,j,k}{}^{2}} + \overline{\tilde{\eta}^{n}_{i,j,k}{}^{(s)^2}} \tag{6}$$

where the overbars on the right hand side are introduced completely analogously to the definition in equation (3). Keeping in mind that $\hat{\eta}$ is independent of the variability from one member to another, then $\overline{\hat{\eta}^2}/\sigma^2_\eta$ is an estimate of the fraction of deterministic variability. The nondeterministic variability fraction is then given by $\overline{\tilde{\eta}^2}/\sigma^2_\eta$. Although the accuracy of these estimates depends on the number of ensemble members, four is sufficient for our purposes where high accuracy is not required.

[32] The fraction of nondeterministic variability of the model SSH is displayed in Figure 3 for the eastern half of the full domain. We note that for the main wave guides in this region, which are the equator and the coast, the SSH variability is largely deterministic. In a section from Baja California to California and a section in the Gulf of Alaska, the nondeterministic variability of the SSH along the coast increases relatively rapidly in the off-coast direction. Nevertheless, even these regions exhibit a high degree of determinism in SSH at grid points adjacent to land. For these coastal grid points, the fraction of nondeterministic

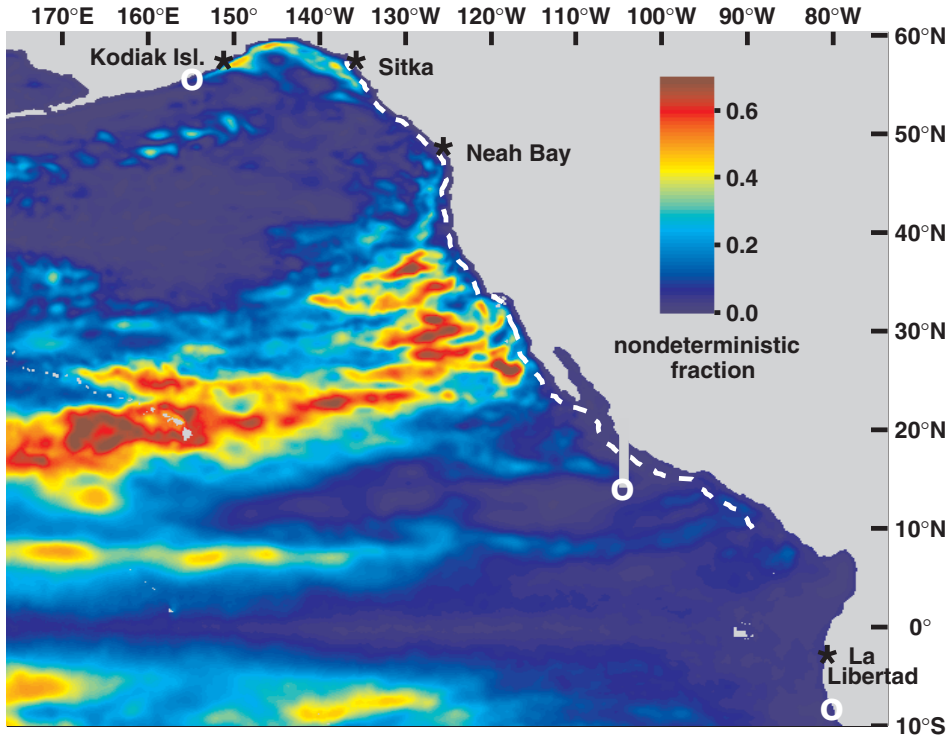

Figure 3. Deterministic versus nondeterministic sea surface height variability in the full domain case. Low and high values indicate high and low degrees of determinism, respectively. These results are based on an ensemble of four simulations, which differ in the initial states only. The white circles at the coast indicate the end points of the longshore lines for which results are displayed by the Hovmøller diagrams in Figures 4 and 6. The RDM was constrained by an artificial coastline at the 104°W meridian, as indicated by the vertical gray line just south of 20°N in this figure. Positions where coastal sea levels were extracted from the model results are indicated by asterisks. The dashed white line shows a distance of four deformation radii from the coast. The color scale used for values of $\overline{\tilde{\eta}^2}/\sigma_{\tilde{\eta}}^2$ (defined in equation (3)) is shown by the bar.

variability ranges from around 0.05 at tropical latitudes to 0.005 or less in the Gulf of Alaska. The length scale of the transition from the coastal regions with mostly deterministic SSH to the open ocean regions with a relatively low degree of determinism is roughly equal to the internal Rossby radius of deformation. On the basis of an estimated propagation speed of 2.5 m/s, the deformation radius varies from approximately 20 km in the GoA to about 100 km at 10°N.

[33] The amplitude of mesoscale variability is small near the boundary because of the constraint on quasi-geostrophic flow that requires stream function invariance along a closed boundary segment. This is consistent with the results in Figure 3. When coastally trapped wave energy radiates offshore as Rossby waves [*Clarke*, 1983; *Johnson and O'Brien*, 1990; *Jacobs et al.*, 1994], the boundary constraint no longer applies and the motion can become unstable. See *Spall* [2000] on the stability of meridional currents and *Thomson and Gower* [1998] on a large observed eddy outbreak in the Gulf of Alaska.

5. Coastal Sea Levels

[34] The objective of this section is to describe the interannual variability of the coastal SLs in the northeast Pacific (NeP) and in the Gulf of Alaska. We define "interannual variability" as the signal that remains after application of a 1-year low-pass boxcar filter to the nonseasonal variability. The boxcar filter was applied to 121 consecutive values, with a time span of 366 days from the first to the last sampled value. The "nonseasonal variability" is found by subtraction of the daily climatology, so there is only a very weak side lobe effect associated with the 1-year filter.

5.1. Methods

[35] SL results from the NLOM simulations were extracted along the coast of the American continent for all ocean grid points that had a neighboring land node. The southernmost positions that were considered, were 8°S, 80°W (near Trujillo, Peru) for the full domain, and 14°N, 104°W (near Manzanillo, Mexico) for the reduced domain, respectively. The boundary sampling ended in the northwest at 56°N, 155°W (slightly west of Kodiak Island, Alaska). These end points of the coastal sections are displayed by white circles in Figure 3. The results presented here were obtained from the period 18 January 1982 through 27 January 1999.

[36] In Figure 4, space-time variations of the nonseasonal SL anomalies at the Pacific Ocean coastline of the American continent are displayed as Hovmøller diagrams

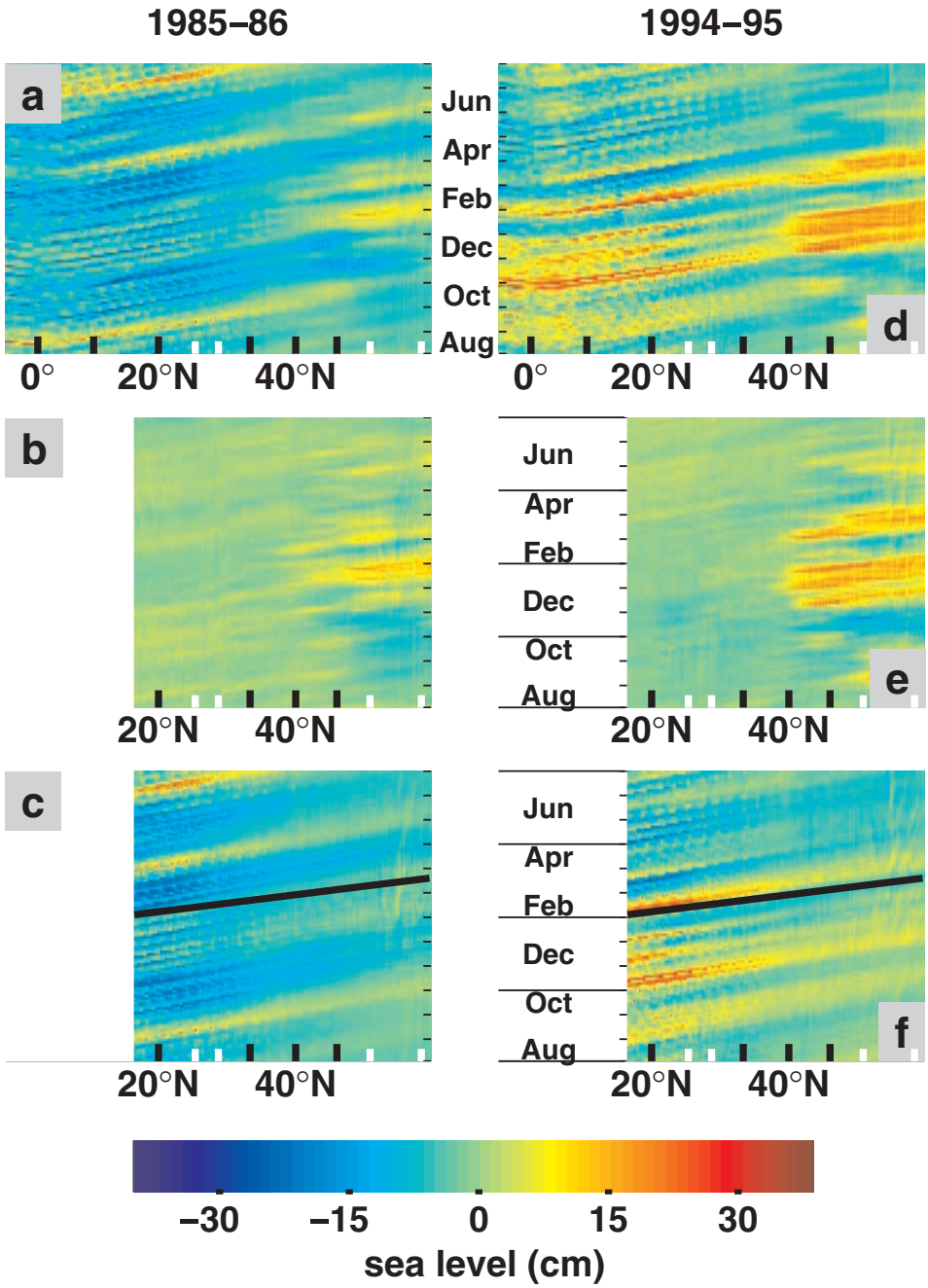

Figure 4. Hovmøller diagrams for SL anomalies extracted along the coastline for the periods August 1985 to July 1986 and August 1994 to July 1995. The climatological seasonal cycle has been removed. Black tick lines on the horizontal axes are latitudes along the coastline, in multiples of 10°. Every second black tick line is labelled. The four white tick lines show the model positions, from left to right, of the northern extent of the Gulf of California, the tip of Baja California, Sitka, and Kodiak Island, respectively. The vertical axes correspond to time, with horizontal lines for the beginning of every third month (the length of the horizontal lines correspond to missing data along the chosen FDM coastline segment). Tick lines along the vertical axes show the beginning of each month. The displayed results are from (a)/(d) the full domain model and (b)/(e) the reduced domain model, respectively. (c)/(f) The SSH differences between the two models are shown, with positive values when the full domain SSH is larger than the reduced domain SSH. The black lines in the center of Figures 4c and 4f have an inclination that corresponds to a propagation speed of 2.5 m/s. The color scale used for SSH values and SSH differences is shown by the bar.

Table 2. Validation of Model Sea Levels[a]

	FDM Versus Observations		RDM Versus Observations		FDM-RDM Versus Observations	
	Correlation	RMS, cm	Correlation	RMS, cm	Correlation	RMS, cm
La Libertad	0.872	2.83				
Neah Bay	0.940	1.30	0.598	3.01	0.804	2.21
Sitka	0.855	1.90	0.554	2.60	0.708	2.43
Kodiak Island	0.775	2.08	0.635	2.02	0.483	2.99

[a]Correlations and root mean square (RMS) differences between observations and model results, after a 1-year low-pass boxcar filter has been applied. Linear trends were removed from all time series prior to the analysis.

for the periods August 1985 to July 1986 and August 1994 to July 1995. Note that the ''coastline'' axes in the Hovmøller diagrams are uniform in coastal grid node numbers, not in latitude. This is particularly noteworthy between 20°N and 30°N, which is a coastline segment that contains the Gulf of California. Also, there is a long coastline segment north of 50°N since the model coast in the GoA is entirely south of 60°N.

[37] In both simulations there are fall and winter SL maxima north of 40°N, of about 10 cm and 20 cm in 1985–1986 and 1994–1995, respectively (yellow and red patches in Figures 4a/4d and 4b/4e). These high SL values are due to the strong regional coastal winds, and are not forced remotely by an oceanic teleconnection. When the RDM SL results are subtracted from the corresponding FDM results, the maxima vanish (Figures 4c and 4f). It is evident that the coastally trapped waves that are generated at equatorial latitudes dominate the SL differences along the coast. These results are representative for the entire simulation period, and they demonstrate that the FDM and RDM simulations are well suited for an examination of remotely forced SL variability along the coast of the NeP and the GoA.

5.2. Discussion

[38] Depictions of the various ISL time series for La Libertad and for one of the stations in the GoA (Sitka) are presented in Figure 2. We note that the peaks in the ISL records for La Libertad are much larger than the corresponding peaks for Sitka, and this is particularly the case during the major El Niño events in 1982–1983 and 1997–1998. This is what one would expect from a coastally trapped signal: When an equatorial Kelvin wave reaches the South American coast, its energy splits. Rossby waves in the Northern Hemisphere are excited south of a critical latitude, and north of this latitude, motion becomes trapped to the coast [*Clarke*, 1983; *Clarke and Shi*, 1991]. Hence, despite net viscous dissipation the amplitude of the equatorial SL signal at the coast is well maintained along the NeP/GoA coastline, which is north of the critical latitude. Figure 2 also suggests that the observed SLs at Sitka are more attenuated than the SL record from the FDM, which misses any attenuation due to dissipation in shallow water.

[39] We note that the FDM results are closer to the observations than the RDM results, with the notable exception of a period of about three years, from 1988 to 1991: During 1988–1989, the RDM record is much closer to the observations than the FDM record, and during 1990–1991 both model records agree closely with the observations. The start of this period coincides with the most prominent La Niña event during the period that is examined here.

[40] Results from a validation of ISL model results versus ISL observations are listed in Table 2. Also included are results for the remotely forced constituent due to oceanic teleconnections, as represented by the difference between the FDM results and the RDM results. The correlations with the observational records are higher for the FDM results than for the RDM results. This indicates that the FDM is superior to the RDM when it comes to reproducing the ISL variability along the NeP/GoA coastline, at least as far north as Sitka.

[41] The trends and standard deviations of the time series are presented in Table 3. The negative trends in the observations along the NeP/GoA coastline are similar to those reported by *Zervas* [2001] and are primarily caused by displacements of the instruments due to vertical crustal movement associated with the post glacial rebound. The magnitude of the positive trends in the NeP/GoA ISLs from the FDM are unrealistic, and they may be related to the rising trend at the equator that is seen both in the observations and in the FDM results. In this investigation, all linear trends have been removed from all time series.

[42] While the standard deviation of the FDM record is close to the observations for Neah Bay, the FDM variability at Sitka and Kodiak Island are higher than the observed variability. This is a quantification of our observation from Figure 2 of more attenuation in the observational record. We also note that the RDM variability is lower than the observed variability for all stations, but that the values from the RDM are approaching realistic levels in the GoA.

[43] In Figure 5, the correlations between the various ISL records at Sitka and the corresponding time series for La Libertad, are depicted as functions of time lag. Interestingly,

Table 3. Trends and Standard Deviations of the Detrended Interannual Sea Level Records

	Observations	Inverted Barometer	FDM	RDM
		Trend, cm/yr		
La Libertad	0.318	− 0.003	0.119	
Neah Bay	− 0.213	0.038	0.287	0.100
Sitka	− 0.269	0.039	0.267	0.091
Kodiak Island	− 1.115	0.023	0.254	0.061
		Standard Deviation, cm		
La Libertad	5.12	0.72	5.75	
Neah Bay	3.68	1.24	3.76	1.57
Sitka	3.11	1.18	3.67	2.02
Kodiak Island	2.53	1.78	3.28	2.13

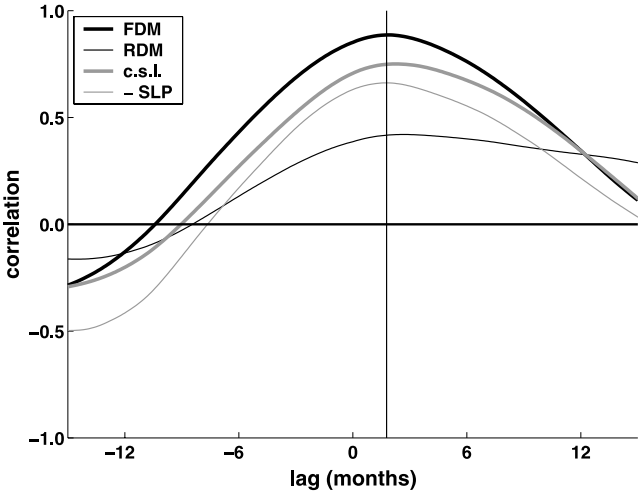

Figure 5. Correlation between interannual sea level anomalies at Sitka and La Libertad, as a function of lag in months. The thick gray line labeled "c.s.l." depicts the correlations based on observations that have been corrected for the inverted barometer effect. The thin gray line shows the results for the lagged correlations between the inverted barometer for Sitka and the corrected sea levels from La Libertad. Thick and thin black lines correspond to FDM and RDM results for Sitka, respectively. (The model results for Sitka SL were correlated with the FDM results at La Libertad.) Lags are positive when the sea levels at La Libertad lead the results for Sitka. The vertical line corresponds to the estimated lag based on a propagation speed of 2.5 m s^{-1} corresponding to 54 days at Sitka.

the correlations from the observations, from the FDM results, and from the inverted barometer, all attain their maximum correlation at approximately the same lag. The differences between the FDM and RDM results also peak at this lag (not shown). Hence both the atmospheric and oceanic teleconnections from the tropical latitudes appear to give rise to remotely forced interannual variability with a lag of 1 1/2–2 months.

[44] The results for the nonseasonal SL anomalies along the American continent during the notable El Niño events in 1982–1983 and 1997–1998 are displayed in Figure 6. The large SL anomalies in fall and winter due to local winds are again eliminated by subtraction of the RDM results from the FDM results. The duration and amplitude of extreme anomalies are shorter and weaker north of 40°N than south of 30°N. In Figures 6c and 6f, where the RDM SL results have been subtracted from the FDM results, we observe signals north of 50N with a magnitude of about 20 cm that are due to remote oceanic forcing during these El Niño events. From Figure 2, similar deductions can be made for the ISL variability during these El Niño events, although the amplitudes are obviously reduced after the 1-year boxcar filter has been applied.

[45] In order to examine relations between El Niño events and interannual variability of the regional atmospheric pressure in the GoA, lagged correlations between the detrended ISLs at La Libertad and the interannual component of the inverted barometer effect were calculated. These results and the corresponding results for the complementary detrended time series of ISLs from the NeP/GoA observations, are presented in Table 4. (As described in section 3, ISLs have been corrected by subtracting the inverted barometer effect from the observed data.) The lags that are listed for the various stations in the Table 4 caption were calculated from a coastal location in the Northern Hemisphere that has an equal distance to the equator as La Libertad. We find that the correlations obtained for the NeP/GoA ISLs are of similar magnitudes as those obtained from the corresponding inverted barometer records. However, from Table 3, we note that the variability of the inverted barometer record is much smaller than the ISL variability.

[46] From the results in Table 5, we find that the lagged correlations between the ISLs at La Libertad in the south and the NeP/GoA tide gauge stations in the north are higher in the FDM than in the observational records. These records and the model results all indicate that El Niño events have a significant impact on the NeP/GoA ISLs, since all lagged correlations drop when the major El Niño events in 1982–1983 and 1997–1998 are excluded from the analysis.

[47] For the full period, the lagged ISL correlation values in Table 5 that are based on results from the RDM are all positive, but the values are significantly lower than the corresponding results from the observations, and from the FDM results. However, when the interim period from July 1983 to June 1997 is considered, any relations between the equatorial ISLs in the FDM integration, and the regional ISLs along the NeP/GoA coastline in the RDM, vanish. Hence the results in Table 5 are consistent with earlier studies which find that, for strong El Niño events, the regional wind forcing plays a role for the ISLs in the NeP/GoA. However, Table 3 reveals that the variability of the ISLs from the RDM integration is considerably lower than the corresponding values from the FDM. We also note that the RDM correlation values in Table 5 are significantly lower than those obtained from the observational records.

[48] The observational evidence that is presented in Tables 3 and 4 is consistent with a strong effect of local atmospheric forcing on the Kodiak Island ISLs, whereas the ISLs at Sitka and Neah Bay are only moderately affected by the local forcing. The model results indicate that the ISLs can predominantly be linked to remote oceanic forcing along the entire coastline of North America. However, from the rightmost column in Table 5, it appears that the remotely forced coastally trapped signal in the model is much less attenuated from Sitka to Kodiak Island than the observational records show. The relatively unattenuated signal due to remote forcing in the model results also yields large error growth and rapidly decreasing correlation values from Sitka to Kodiak Island, as is evident from the results in the two rightmost columns of Table 2.

[49] In this section, we have referred to the signal that we discuss as "coastally trapped". However, this baroclinic signal extends to levels that are deeper than the shelf depth, and is thus trapped to the shelf break. Thus this signal will give rise to a largely barotropic response on the shelf. The barotropic adjustment to the baroclinic forcing will be intricate because of the differences in timescales. The shelf width is a spatial scale that will influence the barotropic response. Moreover, a leakage of energy from the deep ocean to the shelf will affect the amplitude of the propagat-

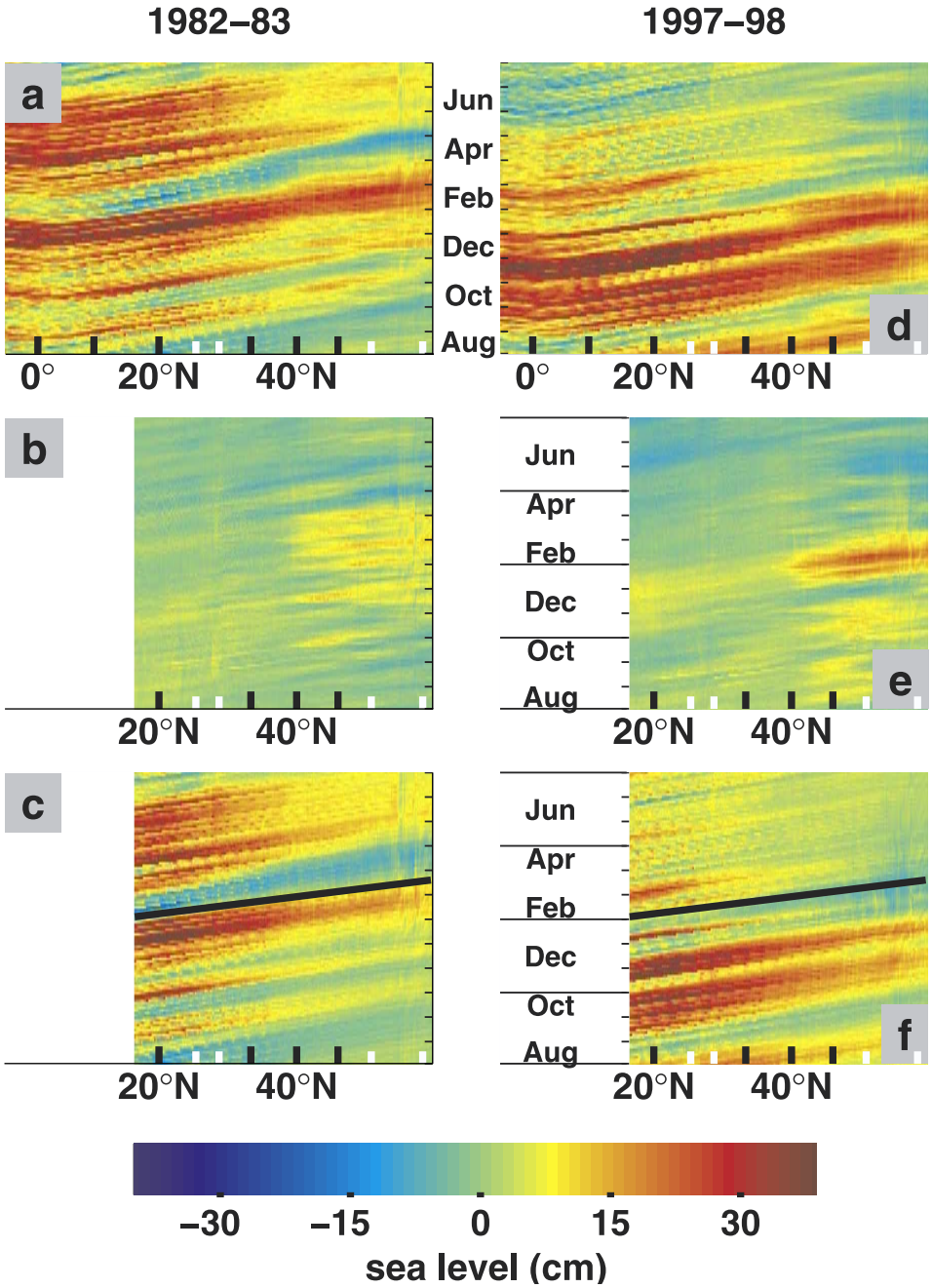

Figure 6. Same as Figure 4 but for the periods (left) August 1982 to July 1983 and (right) August 1997 to July 1998: (a)/(d) From the FDM, (b)/(e) from the RDM, and (c)/(f) the difference between the FDM and the RDM results.

ing baroclinic signal. Hence it is likely that the separation between the tide gauge stations and their model representation at the shelf break will affect the results of the validation.

6. Sea Surface Height Variability

[50] The objective of this section is to describe the interannual variability of the mesoscale intensity in the Gulf of Alaska on the basis of results from the NLOM simulations and on the basis of interpolated fields from altimeter data. Using a comparison of results from the FDM and the RDM simulations, we discuss the impacts of remote oceanic forcing in this context. Our investigation is motivated by the fact that the majority of the previous studies of eddies in the GoA describe such eddies in the context of one or more events. One notable exception is the recent work by *Okkonen et al.* [2001], and they also examine relations between eddies and the regional wind forcing.

6.1. Methods

[51] Formation of eddies is a result of nonlinear processes, often including flow instabilities. Hence application of the method of subtracting the RDM results from the

Table 4. Lagged Correlations Between Interannual Sea Level Observations in the Northeast Pacific Ocean/Gulf of Alaska and Interannual Observations at La Libertad, Ecuador[a]

	Neah Bay	Sitka	Kodiak Island
Corrected sea levels	0.707	0.741	0.510
Inverted barometer	0.573	0.669	0.721

[a]Correlation values are given at lags corresponding to a propagation speed of 2.5 m s^{-1}. The lags then become 48 days, 54 days, and 60 days for Neah Bay, Sitka, and Kodiak Island, respectively. The label "corrected sea levels" refers to results that were obtained on the basis of observations that have been corrected for the inverted barometer effect. The label "inverted barometer" refers to results that were obtained when only this effect was taken into account for the northeast Pacific Ocean/Gulf of Alaska stations, while the corrected interannual SLs from La Libertad were retained.

FDM results for the purpose of identifying the impact of remote forcing on open ocean SSH will not be pursued in this section.

[52] Direct observations of the mesoscale velocity field with the appropriate resolution, duration and extent in time and space are not available for this study. The most comprehensive validation of the mesoscale activity in the FDM members and in the RDM is achieved using altimeter data for SSH anomalies. We might add the mean SSH field to the data and compute the geostrophic currents and the eddy kinetic energy (EKE). The alternative analysis, which is adopted here, is to compare the simulated and observed SSH variability directly. Note that if the mean SSH field in question is constant, the EKE as defined by the square of the velocity anomaly may be derived directly from the SSH anomalies, provided that the assumption of geostrophic motion holds.

[53] Since the magnitude of geostrophic velocities is proportional to the pressure gradient, anomalies associated with the SSH derivative is the natural choice for estimating the EKE. However, in this study we will use anomalies of the actual SSH fields as a measure for the mesoscale intensity. Thus large eddies will yield higher values of this EKE proxy than small eddies with the same velocities. Our approach has been adopted to facilitate validation of the model mesoscale by the SSH records from satellite altimeter data: Because of the relatively coarse horizontal resolution of the altimeter data, the interpolated SSH fields will devaluate the contribution from small eddies to the mesoscale intensity [*Jacobs et al.*, 2001].

[54] The analysis of mesoscale variability in section 6.2 below has been conducted as follows: For each time record, results were extracted in bands that are parallel to the model coastline. (The interpolated altimeter data in regions were the ocean depth is less than 200 m were disregarded.) The region of interest was defined as the eastern GoA limited by 48°N in the south and 143°W in the west, see Figure 7a. Then, for each band and each record, a linear least squares fit to the SSH values was calculated. Finally, the root mean square (RMS) differences between the results and the best fit line for each band were used as a proxy for the mesoscale intensity; an example is provided in Figure 7b. The rationale for this is that for a cross section of an eddy, the sea surface elevation will appear as an undulation superimposed on the large scale tilt. The tilt of the best fit line is a measure of the large-scale circulation's component perpendicular to the line.

[55] Each band has a width of one grid node, and the bands are binned together in groups of eight. The width of each group of bands then becomes about 100 km. Two such groups of bands are displayed by gray shaded regions in Figure 8c. These groups of bands will hereafter be referred to as "Region I" and "Region II".

6.2. Discussion

[56] Results for the low-pass filtered RMS offsets from the RDM and from two members of the FDM are displayed in Figures 8a and 8b. A careful examination of the results reveals that the peaks in the RMS differences in Region I closest to the coast lead the values in Region II farther away from the coast. The amplitudes are also generally slightly lower in Region II. This indicates that the proxy measure for the mesoscale intensity captures the off-shore propagation of eddies that attenuate in the direction of propagation.

[57] Furthermore, we observe that the most intense mesoscale activity in the FDM-1 and RDM simulations occurs in 1983 and 1998, i.e., in the aftermath of the two major El Niño events. A third event in 1995 has a similar amplitude in Region I, but is strongly attenuated away from the coast. These results suggest that strong ENSO events have a significant impact on the mesoscale ocean circulation in the eastern GoA. Moreover, in late 1982 through 1983 and in late 1997 through 1998 the results from the simulations are strikingly similar. Hence, while the teleconnections by an oceanic pathway are clearly significant for the coastal SL anomalies (section 5), our results indicate that the tele-

Table 5. Interannual Sea Levels in the Northeast Pacific Ocean/Gulf of Alaska Versus Interannual Sea Levels at La Libertad[a]

	Observations Versus Obs. at La Libertad	FDM Results Versus FDM at La Libertad	RDM Results Versus FDM at La Libertad	FDM - RDM Versus FDM at La Libertad
		Period: Jan. 1982 to Dec. 1998		
Neah Bay	0.707	0.953	0.469	0.879
Sitka	0.741	0.887	0.412	0.877
Kodiak Island	0.510	0.835	0.265	0.874
		Period: July 1983 to June 1997		
Neah Bay	0.364	0.861	− 0.010	0.781
Sitka	0.598	0.725	0.082	0.779
Kodiak Island	0.217	0.651	− 0.003	0.776

[a]Correlation values are given for the same lags as in Table 4. All linear trends have been removed, and the sea levels were corrected for the inverted barometer effect.

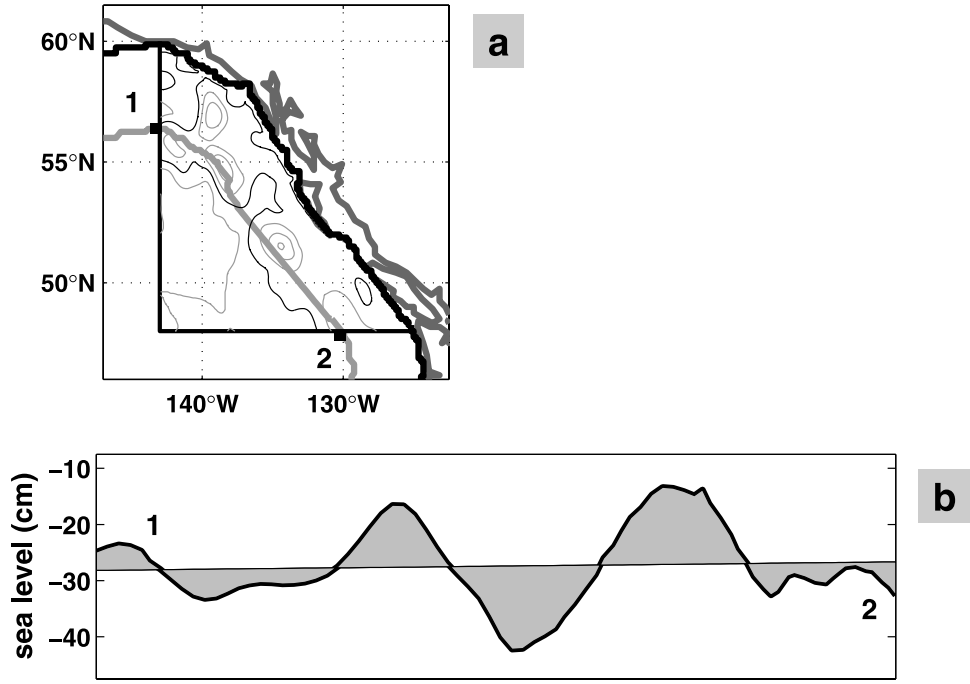

Figure 7. Explanation of how information on the SSH variability is analyzed. Results have been calculated for the region limited by 48°N in the south and 143°W in the west, as indicated by the horizontal and vertical thick black lines in Figure 7a. The SSH values in this region are displayed for one particular date (1 August 1998; FDM) by thin contour lines (one black and a number of gray lines) with a 10 cm contour interval. The black contour line indicates the −40 cm contour. The thick black line and the thick dark gray line display the model coastline and the actual coastline, respectively. The thick light gray line corresponds to a longshore band (band 28 from the coastline; see text). The ends of this band in the specified region are indicated by 1 in the northwest and 2 in the south. The extracted SSH results for band 28 are given by the thick line in Figure 7b. The least squares fit to these SSH results is shown as the straight thin line. In order to quantify the mesoscale variability for this particular date and band the RMS of the differences between these two lines was computed.

connections by an atmospheric pathway dominate the effect on the ocean's mesoscale in the eastern GoA. However, the RMS differences from the FDM members displayed in Figure 8 are generally marginally lower than the results from the RDM. Also, the peaks in the FDM results for 1983 are lagging the RDM peak slightly. These findings may be related to the differences in the daily climatologies of SLs, since the RDM climatology has a somewhat larger amplitude than the FDM climatology, and since the peak in the RDM climatology leads the FDM peak by about one month.

[58] The main deviation in the mesoscale results between the RDM and the FDM-1 occurs during 1985 and 1986 in Region I. The deviation is also quite noticeable in Region II, about one year later. This coincides with a period of relatively strong alongshore local winds [*Melsom et al.*, 1999, Figure 14]. Since the mesoscale eddy activity is more intense in the RDM than in the FDM-1 during this period, our results indicate that on occasion, remotely forced oceanic variability can affect the strength and number of eddies in the eastern GoA. At the time the RDM was in the early stages of GoA eddy development, in the FDM, an upwelling Kelvin wave of equatorial origin reached the GoA, suppressing eddy development.

[59] The results from the FDM-1 and RDM simulations can be compared with results from the interpolated fields of the MODAS product for the overlapping period, see Figure 8d for the results in Region II. In a comparison with surface dynamic height derived from bathythermographs, it has been shown that SSH variability is substantially underrepresented in the MODAS analyses (J. F. Cayula, personal communication). The peaks in 1995 and 1998 in the results from all the simulations are also found in the altimeter data, albeit with smaller amplitudes.

[60] We note that the shape of the 1995 peak is very different in the model results and in the data: The rise in the RMS differences from the MODAS fields is not sustained for more than approximately six months, about half of the duration of the rise in the model simulations. The same relation can be seen for the decline, while the duration of the anomalous RMS differences are about the same in the data as in the model. The results from the altimeter data for 1998 indicate a similar development as in 1995.

7. Summary and Concluding Remarks

[61] In this study we have obtained quantitative measures of the impact of remote oceanic teleconnections due to ENSO events along the GoA coastline and in the interior of the GoA, on interannual timescales. The analysis of deterministic versus nondeterministic variability in section 4

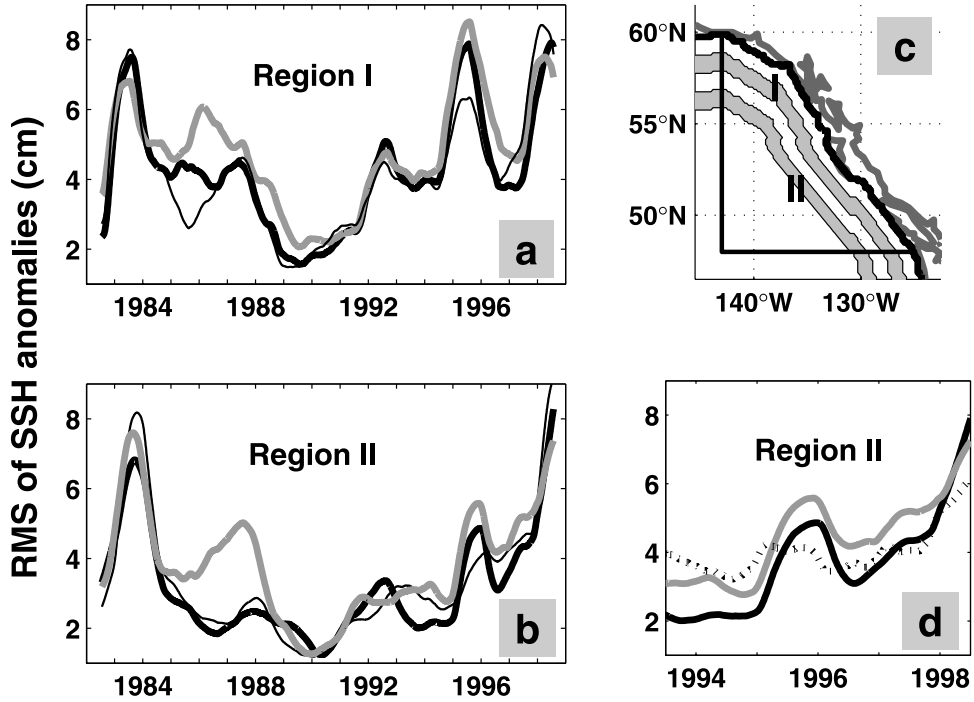

Figure 8. Interannual mesoscale variability in the eastern Gulf of Alaska, based on model output and altimeter data for the SSH. The gray shaded regions in Figure 8c correspond to the two regions for which results are depicted in the other panels. There, RMS offsets of SSH from the linear best fit longshore SSH are depicted, after a 1-year filter was applied. (a) The RMS of offsets for the FDM and the RDM in a region at a distance of 100–200 km from the model coastline (Region I) are displayed. (b) The corresponding results for the region at a distance of 300–400 km from the coastline (Region II) can be viewed. The black lines show results from two members of the FDM, and the gray line corresponds to results from the RDM. (d) The results for Region II are shown, along with results from the altimeter data in the overlapping period. (The altimetry product that has been used starts in 1993.) The results from the altimeter data are depicted by the dotted line, and the results from only one of the FDM members are shown. Tick marks along the horizontal axes indicate the beginning of years. See the text for further details.

revealed that almost all variability at the GoA coast can be attributed to the atmospheric forcing (which can be regional or remote). Nondeterministic variability becomes more important for the mesoscale variability in the interior of the GoA, but in section 6, we defined an integrated measure of interannual mesoscale variability and changes in the integrated variability through time turned out to be only slightly nondeterministic.

[62] Results for the coastal SLs were presented in section 5. From observational records, we found that 50% and 55% of the ISL variances for Neah Bay and Sitka, respectively, can be explained statistically by the equatorial SL data. On the basis of model results that incorporate teleconnections by an oceanic pathway from tropical latitudes, the explained variances become 79% and 91% for these locations, respectively. On the other hand, when the oceanic teleconnections are eliminated and only teleconnections in the atmospheric forcing fields are retained, the model results yield explained variances of about 20%. In section 6 we presented evidence for a significant impact of strong El Niño events on the interannual mesoscale variability in the GoA. However, most of this variability was also manifested when oceanic teleconnections from tropical latitudes were excluded. Hence we suggest that the interannual mesoscale variability in the GoA can largely be attributed to the regional wind forcing. Below, we discuss these findings in the context of relevant existing knowledge prior to this study.

[63] As can be deduced from Figure 5, our results reveal a propagation speed of ISLs along the coast of the American continent of about 2.5 m/s. This is a much faster propagation than the speed of 0.4 m/s that was reported by *Chelton and Davis* [1982]. The fast propagation speed that we find is much closer to the values that have been reported for subannual frequencies, see *Meyers et al.* [1998] and references therein, and also Figures 4 and 6 in this study.

[64] According to our results from the RDM, the ISL variability north of the California coastline cannot to any significant degree be attributed to midlatitude forcing along the section from 24°N (which is the southernmost latitude of unmodified RDM winds) to California. Interestingly, *Spillane et al.* [1987] conclude that the intraseasonal SL signal propagates unforced by local meteorological influences along the coastline segment from 9°N to 54°N. In a recent examination of SL variability at synoptic to annual timescales, *Subbotina et al.* [2001] concludes that remote oceanic effects during the El Niño events in 1982–1983 and 1997–1998 do not propagate beyond central California. North of this region, they attribute changes in SL to

atmospheric variability for the timescales that they consider. In this context, it is interesting to note from our description in section 2 that while the daily climatology of coastal SL from the RDM has an unrealistically large amplitude at 20°N, its magnitude at 55°N is much more credible.

[65] Keeping in mind that the RDM includes regional winds but excludes remote oceanic forcing, we note from Figure 2 that the RDM results for Sitka are closer to the ISL observations during the latter event (although more so in shape than in magnitude). This suggests that atmospheric variability played a greater role in the 1997–1998 event. According to *Subbotina et al.* [2001], the 1997–1998 El Niño had greater variability at synoptic timescales, whereas the 1982–1983 El Niño generated higher signal variance at seasonal scales.

[66] In their study, *Melsom et al.* [1999] suggest that "the deep model eddies generated in early 1983 are predominantly due to oceanic ENSO teleconnections". The present results downplay the role of oceanic teleconnections for the mesoscale activity in the GoA during 1983, since the FDM and RDM results for the mesoscale are similar during 1983, see Figures 8a and 8b. On the basis of model results and observational evidence presented by *Tabata* [1982], *Melsom et al.* [1999] also argue that La Niña events in the equatorial Pacific Ocean suppress eddy activity in the GoA. The analysis in section 6 shows that the weakest mesoscale intensity occurs in 1989, following the strongest La Niña in the simulation period. Near the coast, this minimum is slightly lower in the FDM than in the RDM results.

[67] Using the same numerical model as in this study, *Okkonen et al.* [2001] concluded that the mesoscale variability in the GoA can mainly be attributed to the regional wind forcing near the coast. This finding is in accord with the results presented in section 6 in this study. They note that downwelling associated with a negative wind stress curl near the coast will enhance horizontal and vertical shears, which initially destabilize the Alaska Current and ultimately generate eddies when the current weakens. The winters of 1982–1983 and 1985–1986 are the periods with the most prominent negative wind stress curls [*Okkonen et al.*, 2001, Figure 11] in their simulation. However, during 1986 *Okkonen et al.* [2001] find that there is only moderate mesoscale activity in the GoA. In this context, we note from Figure 8 that the results from the RDM are indicative of strong mesoscale activity in 1986, and the intensity on the mesoscale in Region I (near the coast) is nearly as large in 1986 as in 1983 in the RDM. Moreover, 1986 is the year with the largest differences in the mesoscale results between the RDM on one side and the two FDM members on the other side. Figure 4c discloses that the model results along the coast in late 1985 are modified by an upwelling, coastally trapped wave of tropical origin. Hence this study reveals that remote oceanic forcing may affect the mesoscale circulation in the GoA under certain conditions.

[68] The results in section 6 indicate that 1983, 1995, and 1998 are the years with the strongest mesoscale activity in the GoA. The thermal imagery from the winter and spring of 1983 presented by *Thomson and Emery* [1986] reveals intense mesoscale activity, including meanders and eddies, off the GoA coast from 53°N to 56°N. For 1995, only a moderately strong eddy activity is displayed by the MODAS altimeter data, see Figure 8. However, the thermal imagery from March 1995 that is examined by *Thomson and Gower* [1998] displays an abundance of eddies. The MODAS analyses from 1998 confirm the presence of numerous eddies that are seen in the model results. On the basis of the same altimeter data, the intense mesoscale activity in the GoA during 1998 has previously been reported by *Crawford and Whitney* [1999].

[69] We have presented evidence of a substantial impact of remote oceanic forcing on the ISL along the eastern GoA shoreline. Analysis of simulations of the circulation in the Pacific Ocean has revealed that the agent of this remote forcing is oceanic ENSO variability, which is conveyed by coastally trapped waves. The propagating signal in the model results has been compared with observed SLs, and the records from La Libertad (Equador), Neah Bay (WA), and Sitka (AK), are consistent with our conclusion. The intensity in eddy activity in the eastern GoA can also be linked to ENSO variability, predominantly by remote atmospheric forcing.

[70] **Acknowledgments.** This work has been supported by the Norwegian Research Council under contracts 122230/720 and 146476/120. Funding for NRL participation is provided by the Office of Naval Research under the project 6.1 Dynamics of Low Latitude Western Boundary Currents (Program element 61153N). We are grateful for their support. Sea level data were obtained from the University of Hawaii Sea Level Center (http://uhslc.soest.hawaii.edu/) and from the National Oceanic and Atmospheric Administration Center for Operational Oceanographic Products and Services (NOAA CO-OPS, http://www.co-ops.nos.noaa.gov/). The numerical simulations were performed using computer time grants from the U.S. Department of Defense High Performance Computing Modernization Program and were run on the Cray T3E at the U.S. Army Engineer Research and Development Center in Vicksburg, Mississippi. The MODAS SSH analyses were processed from altimeter data by Charlie N. Barron Jr (NRL). The study was initiated on the basis of ideas and suggestions made by James J. O'Brien (Florida State University). The concept for the reduced domain model (RDM), subsequently elaborated by one of us (EJM), was originally suggested by Steven D. Meyers (University of South Florida). We are indebted to their generous contributions. We would also like to thank Stephen R. Okkonen (University of Alaska Fairbanks) and an anonymous reviewer for their helpful comments and suggestions. This paper is NRL contribution number NRL/JA/7320/02/0006.

References

Bhaskaran, S., G. S. E. Lagerloef, G. H. Born, W. J. Emery, and R. L. Leben, Variability in the Gulf of Alaska from Geosat altimeter data, *J. Geophys. Res.*, *98*, 16,311–16,330, 1993.

Bjerknes, J., A possible response of the atmospheric Hadley circulation to anomalies of ocean temperature, *Tellus*, *18*, 820–829, 1966.

Chelton, D. B., and R. E. Davis, Monthly mean sea-level variability along the west coast of North America, *J. Phys. Oceanogr.*, *12*, 757–784, 1982.

Chelton, D. B., and D. B. Enfield, Ocean signals in tide gauge records, *J. Geophys. Res.*, *91*, 9081–9098, 1986.

Clarke, A. J., The reflection of equatorial waves from oceanic boundaries, *J. Phys. Oceanogr.*, *13*, 1193–1207, 1983.

Clarke, A. J., and C. Shi, Critical frequencies at ocean boundaries, *J. Geophys. Res.*, *96*, 10,731–10,738, 1991.

Crawford, W. R., and F. A. Whitney, Mesoscale eddy aswirl with data in Gulf of Alaska, *Eos Trans. AGU*, *80*(33), 365, 370, 1999.

Emery, W. J., and K. Hamilton, Atmospheric forcing of interannual variability in the northeast Pacific Ocean: Connections with El Niño, *J. Geophys. Res.*, *90*, 857–868, 1985.

Enfield, D. B., and J. S. Allen, On the structure and dynamics of monthly mean sea level anomalies along the Pacific coast of North and South America, *J. Phys. Oceanogr.*, *10*, 557–578, 1980.

European Centre for Medium-Range Weather Forecasts (ECMWF), User guide to ECMWF products, *Meteorol. Bull. M3.2*, Reading, UK, 1995.

Fox, D. N., W. J. Teague, C. N. Barron, M. R. Carnes, and C. M. Lee, The Modular Ocean Data Assimilation System (MODAS), *J. Atmos. Oceanic Technol.*, *19*, 240–252, 2002.

Gibson, J. K., P. Kållberg, S. Uppala, A. Hernandez, A. Nomura, and E. Serrano, ERA description, *ECMWF Re-anal. Proj. Rep. Ser. 1*, 72 pp., Eur. Cent. for Medium-Range Weather Forecasts, Reading, UK, 1997.

Hellerman, S., and M. Rosenstein, Normal monthly wind stress over the world ocean with error estimates, *J. Phys. Oceanogr.*, *13*, 1093–1104, 1983.

Hsieh, W. W., M. K. Davey, and R. C. Wajsowicz, The free Kelvin wave in finite-difference numerical models, *J. Phys. Oceanogr.*, *13*, 1383–1397, 1983.

Hundermark, B. W., H. E. Hurlburt, E. J. Metzger, and J. F. Shriver, A comparison of wind stresses derived from archived operational ECMWF 1000 mb winds and FSU pseudo stresses over the tropical Pacific Ocean, 1981–93, *NRL/FR/7320-99-9643*, 40 pp., Nav. Res. Lab., Stennis Space Cent., Miss., 1999.

Hurlburt, H. E., and J. D. Thompson, A numerical study of Loop Current intrusions and eddy shedding, *J. Phys. Oceanogr.*, *10*, 1611–1651, 1980.

Hurlburt, H. E., A. J. Wallcraft, W. J. Schmitz Jr., P. J. Hogan, and E. J. Metzger, Dynamics of the Kuroshio/Oyashio current system using eddy-resolving models of the North Pacific Ocean, *J. Geophys. Res.*, *101*, 941–976, 1996.

Jacobs, G. A., H. E. Hurlburt, J. C. Kindle, E. J. Metzger, J. L. Mitchell, W. J. Teague, and A. J. Wallcraft, Decade-scale trans-Pacific propagation of an El Niño anomaly, *Nature*, *370*, 360–363, 1994.

Jacobs, G. A., C. N. Barron, and R. C. Rhodes, Mesoscale characteristics, *J. Geophys. Res.*, *106*, 19,581–19,595, 2001.

Jacobs, G. A., C. N. Barron, D. N. Fox, K. R. Whitmer, S. Klingenberger, D. May, and J. P. Blaha, Operational altimeter sea level products, *Oceanography*, *15*, 13–21, 2002.

Johnson, M. A., and J. J. O'Brien, The northeast Pacific Ocean response to the 1982–1983 El Niño, *J. Geophys. Res.*, *95*, 7155–7166, 1990.

Lagerloef, G. S. E., Interdecadal variations in the Alaska Gyre, *J. Phys. Oceanogr.*, *25*, 2242–2258, 1995.

Matthews, P. E., M. A. Johnson, and J. J. O'Brien, Observation of mesoscale ocean features in the northeast Pacific using Geosat radar altimetry data, *J. Geophys. Res.*, *97*, 17,829–17,840, 1992.

Melsom, A., S. D. Meyers, H. E. Hurlburt, E. J. Metzger, and J. J. O'Brien, ENSO effects on Gulf of Alaska eddies, *Earth Interactions*, *3*, 1–30, 1999. (Available as http://EarthInteractions.org)

Metzger, E. J., and H. E. Hurlburt, The nondeterministic nature of Kuroshio penetration and eddy shedding in the South China Sea, *J. Phys. Oceanogr.*, *31*, 1712–1732, 2001.

Metzger, E. J., H. E. Hurlburt, J. C. Kindle, Z. Sirkes, and J. M. Pringle, Hindcasting of wind-driven anomalies using a reduced gravity global ocean model, *Mar. Technol. Soc. J.*, *26*, 23–32, 1992.

Metzger, E. J., H. E. Hurlburt, G. A. Jacobs, and J. C. Kindle, Hindcasting wind-driven anomalies using reduced-gravity global ocean models with 1/2° and 1/4° resolution, *NRL Tech. Rep. 9444*, 21 pp., Nav. Res. Lab., Stennis Space Center, Miss., 1994.

Meyers, S. D., A. Melsom, G. T. Mitchum, and J. J. O'Brien, Detection of the oceanic fast Kelvin wave teleconnection during ENSO, *J. Geophys. Res.*, *103*, 27,655–27,663, 1998.

Moore, D. R., and A. J. Wallcraft, Formulation of the NRL Layered Ocean Model in spherical coordinates, *NRL/CR/7323-96-0005*, 24 pp., Nav. Res. Lab., Stennis Space Center, Miss, 1998.

Murray, C. P., S. L. Morey, and J. J. O'Brien, Interannual variability of upper ocean vorticity balances in the Gulf of Alaska, *J. Geophys. Res.*, *106*, 4479–4491, 2001.

National Oceanic and Atmospheric Administration, ETOP05 digital relief of the surface of the Earth, *Data Announce. 86-MGG-07*, Natl. Geophys. Data Cent., Boulder, Colo., 1986.

O'Brien, J. J., and F. Parham, Equatorial Kelvin waves do not vanish, *Mon. Weather Rev.*, *120*, 1764–1766, 1992.

Okkonen, S. R., G. A. Jacobs, E. J. Metzger, H. E. Hurlburt, and J. F. Shriver, Mesoscale variability in the boundary currents of the Alaska Gyre, *Cont. Shelf Res.*, *21*, 1219–1236, 2001.

Ramp, S. R., J. L. McClean, C. A. Collins, A. J. Semtner, and K. A. S. Hays, Observations and modeling of the 1991–1992 El Niño signal off central California, *J. Geophys. Res.*, *102*, 5553–5582, 1997.

Royer, T. C., Seasonal variations of waters in the northern Gulf of Alaska, *Deep Sea Res.*, *22*, 403–416, 1975.

Spall, M. A., Generation of strong mesoscale eddies by weak ocean gyres, *J. Mar. Res.*, *58*, 97–116, 2000.

Spillane, M. C., D. B. Enfield, and J. S. Allen, Intraseasonal oscillations in sea level along the west coast of the Americas, *J. Phys. Oceanogr.*, *17*, 313–325, 1987.

Subbotina, M. M., R. E. Thomson, and A. B. Rabinovich, Spectral characteristics of sea level variability along the west coast of North America during the 1982–83 and 1997–98 El Niño events, *Prog. Oceanogr.*, *49*, 353–372, 2001.

Tabata, S., The anticyclonic, baroclinic eddy off Sitka, Alaska, in the northeast Pacific Ocean, *J. Phys. Oceanogr.*, *12*, 1260–1282, 1982.

Teague, W. J., M. J. Carron, and P. J. Hogan, A comparision between the Generalized Digital Environmental Model and Levitus climatologies, *J. Geophys. Res.*, *95*, 7167–7183, 1990.

Thomson, R. E., and W. J. Emery, The Haida current, *J. Geophys. Res.*, *91*, 845–861, 1986.

Thomson, R. E., and J. F. R. Gower, A basin-scale oceanic instability event in the Gulf of Alaska, *J. Geophys. Res.*, *103*, 3033–3040, 1998.

Wallcraft, A. J., The Navy Layered Ocean Model users guide, *NOARL Rep. 35*, 21 pp., Nav. Oceanogr. Lab., Stennis Space Center, Miss., 1991.

Wallcraft, A. J., and D. R. Moore, The NRL Layered Ocean Model, *Parallel Comput.*, *23*, 2227–2242, 1997.

Zervas, C. E., Sea level variations of the United States 1854–1999, *NOAA Tech. Rep. NOS CO-OPS 36*, 187 pp., Natl. Oceanic and Atmos. Admin., Silver Spring, Md., 2001.

H. E. Hurlburt and E. J. Metzger, Ocean Dynamics and Prediction, Naval Research Laboratory, Stennis Space Center, MS 9529-5004, USA. (hurlburt@nrlssc.navy.mil; metzger@nrlssc.navy.mil)

A. Melsom, Norwegian Meteorological Institute, P.O. Box 43 Blindern, NO-0313 Oslo, Norway. (arne.melsom@met.no)